Photosystem II as a chemiluminescence-induced photosensitizer for photoelectrochemical biofuel cell-type biosensing system

Bekir Çakıroğlu, Naiba Jabiyeva, Michael Holzinger

Photosystem II as a chemiluminescence-induced photosensitizer for photoelectrochemical biofuel cell-type biosensing system

Bekir Çakıroğlu[a,b]*, *Naiba Jabiyeva*[a,c], *Michael Holzinger*[a,d]*

[a]*Université Grenoble Alpes, DCM UMR 5250, F-38000, Grenoble, France*

[b]*Sakarya University, Biomedical, Magnetic and Semiconductor Materials Research Center (BIMAS-RC), 54187 Sakarya, Turkey*

[c]*Sakarya University, Science & Arts Faculty, Department of Chemistry, 54187 Sakarya, Turkey*

[d]*CNRS, DCM UMR 5250, F-38000, Grenoble, France*

*Corresponding Author. Tel.: +90 264 295 31 84

E-mail address: bekircakiroglu@sakarya.edu.tr (B.Çakıroğlu).

*Corresponding Author. Tel.: +33 (0)4.56.52.08.11; Fax: +33 (0)4.56.52.08.05

E-mail address: michael.holzinger@univ-grenoble-alpes.fr

ABSTRACT:

Herein, photosystem II (PSII), extracted from spinach, is used for the first time as an efficient and green sensitizer for a photobioanode in a photoelectrochemical glucose biofuel cell (PBFC) setup. The concept is based on the formation of hemin-catalyzed luminol chemiluminescence (CL) after the enzymatic oxidation of glucose and the simultaneous production of hydrogen peroxide by glucose oxidase. The photosynthetic enzyme PSII, combined with an osmium polymer serving as mediator and photosensitizer, is immobilized and wired on microporous carbonaceous material (MC) for the chemiluminescence-induced oxidation of water to O_2 at the photobioanode (GCE|MC|Os polymer|PSII). Also, bilirubin oxidase immobilized on multiwalled carbon nanotubes (MWCNTs) coated electrode (GCE|MWCNT|BOx) serves as a biocathode. The photoelectrochemical biofuel cell (PBFC) is applied to a biosensor model system to validate the appropriateness of such a bioanode operating in a self-powered mode. Os redox polymer attached to MCs provides abundant PSII immobilization and a reliable electron transfer pathway. The well-matching energy levels of photosensitive entities reduce recombination phenomena while MC enhances the charge collection. Substantial photocatalytic water oxidation was observed under CL due to the well-matched CL emission and PSII absorption. The electrode is rationally designed to gain the maximum luminol CL power for the photobioanode. The open circuit potential of PBFC linearly increased with the CL power intensity and, in turn, glucose concentrations in the range of 0-6 mmol L^{-1}. The PBFC yielded an OCP of 0.531 V in 30 mmolL^{-1} glucose. The study may open a new horizon to the green and pioneering PEC biosensing realm.

KEYWORDS: Photosystem II, Osmium complex, Porous carbonaceous material, Photoelectrochemical biofuel cell, Luminol

1. INTRODUCTION

Photoelectrochemical biofuel cells (PBFCs) include light-assisted bioelectrocatalysis with energy conversion of light and chemical energy to electricity. Its principle combines the aspects of enzymatic BFCs and solar cells (Zhang et al., 2015). A sub-category of Photoelectrochemical (PEC) biosensing systems can operate under a "self-produced" illumination mode and are scarce in the literature. However, in these systems, the sensitivity and selectivity can be enhanced compared to ordinary PEC biosensing systems since the photoresponse is proportional to the chemiluminescence power intensities, and in turn, released H_2O_2 concentration after GOx-catalyzed glucose oxidation (Golub et al., 2012).

PSII is a multi-subunit redox enzyme and catalyzes solar-driven water oxidation during photosynthesis (Dilbeck et al., 2013). Nowadays, there is substantial interest in integrating photosynthetic enzymes such as PSII onto electrodes to assemble futuristic photovoltaic devices, and the photoresponses were boosted with increasing visible light intensities in these ensembles (Badura et al., 2008; Fang et al., 2019; Hasan et al., 2014; Zhang and Reisner, 2020). The immobilization of single monolayer PSII results in limited photocatalytic activity. The photocurrents are generated from the enzymes within a few micrometers of thickness, and the remaining enzymes in the outer layers do not contribute to the photoresponse (Riedel et al., 2018). This problem has been overcome by entrapping PSII in a redox polymer matrix, which increased the immobilized PSII due to the large surface area and enhanced the electron transfer (Kato et al., 2014; Sokol et al., 2016; Yehezkeli et al., 2012). As far to our knowledge, PSII has been utilized only herbicide detection in the biosensor area by detecting PSII inhibition (Wang et al., 2020). Using PSII as a sensitizer in PEC biosensors can expand its application area and contribute to sustainable development of green chemistry.

The refraction angles and wavelengths of the light coming into the atmosphere make the sky blue. Thus, it is quite plausible that PSII has evolved to absorb a stronger blue wavelength range relative to other parts of the light spectrum (Tarakanov et al., 2022). Most studies have focused on the excitation of the red sideband of PSII in PEC systems. However, Willner's research group has found that the photocurrent generation at the blue-side absorption band of PSII (Soret or B-band, 420–440 nm) is three-fold higher than the value at the red-side absorption band (Q-band, ~675 nm) at Au/poly(mercapto-p-benzoquinone)/PSII photobioanode, implying that the excitation of Soret band is clearly more rational for PEC systems (Kato et al., 2014; Yehezkeli et al., 2012). Rao et al. have immobilized PSII extracted

from spinach onto ruthenium complex-sensitized TiO_2-covered electrodes and illuminated them with a 420 nm filter inserted light source (35 mW cm^{-2}), which can excite the blue-side band. The incident photon-to-current efficiency (IPCE) was 12%, with photocurrents up to 35 µA cm^{-2}, reporting one of the highest IPCE for PSII (Gratzel et al., 1990). However, upon illumination under a light source with longer wavelengths (>670 nm), which can only excite the red-side band, IPCEs were lower than 0.3%, according to the literature (Kato et al., 2014). Therefore, the blue-side band harnessing of PSII can be more promising for increasing IPCE in futuristic PEC systems.

Redox polymers play a pivotal role in fabricating reagentless amperometric biosensors and PSII immobilized electrodes (Heller and Feldman, 2008; Sokol et al., 2016). Redox polymers can shuttle electrons between the active site of the redox enzyme and the electrode surface through the hopping mechanism from one redox center to the next on the polymer backbone (Riedel et al., 2018). Osmium complexes are widely used in redox polymers due to their favorable redox potential and photostability compared to ruthenium complexes (Zammit et al., 2012).

Due to their high biocatalytic current generation rates resulting from their supercapacitor nature, advanced carbonaceous structures have been employed extensively in biofuel cells (Cosnier et al., 2016; Gross et al., 2018).

Herein, a **novel "self-illuminating" PBFC** was fabricated using PSII mixed with Os-polymer on microporous carbon as a photobioanode to estimate glucose concentrations by measuring open circuit potentials. The **Soret band of PSII was focused and excited by luminol illumination** for the first time in a PEC biofuel cell, by **trapping PSII in an Os polymer**, which acted as the sensitizer. Luminol chemiluminescence **(CL)** was activated by the enzymatic production of hydrogen peroxide of GOx during glucose oxidation. A good PEC performance was observed due to the following factors ~~as follows~~. 1. The supply of **luminol chemiluminescence** with **perfect emission spectrum for the absorption of PSII** yielded high photocurrents implying the importance of harnessing Soret bands of porphyrin within PSII. 2. The **porous architecture of electron collecting carbonaceous** support allowed stable and abundant PSII loading and Os polymer deposition, which is superior to the flat film supports. 3. PEC activity of osmium polymer contributed to the PEC performance of PSII. Its **energy levels matched well with those of PSII** resulting in the efficient photogenerated electron transfer. Additionally, **PSII with a high water oxidation activity was purified from cheap resource spinach**, which is advantageous compared to other resources.

2. EXPERIMENTAL SECTION

2.1. Materials and Apparatus

GOx (50 KU g^{-1} solid) from *Aspergillus niger* and Bilirubin oxidase (BOx, 15-65 units mg^{-1} protein) from *Myrothecium verrucaria* (Mv) were obtained from Sigma-Aldrich (UK). Monosodium phosphate monohydrate (NaH_2PO_4), disodium hydrogen phosphate heptahydrate (Na_2HPO_4), D-(+)-glucose, 4-Morpholineethanesulfonic acid (MES), 4-(2-hydroxyethyl)-1-piperazineethanesulfonic acid (HEPES), KNO_3, $NaNO_3$, hemin, benzamidine, triton X-100, NaC1, $CaC1_2$, $MgCl_2$, $MgSO_4$, sucrose, n-Dodecyl β-D-maltoside, 2,2'-bipyridyl, K_2OsCl_6, lithium chloride (≥99.0 %), tetrabutylammonium hexafluorophosphate (≥99.0%) ($[Bu_4N]PF_6$), poly(ethylene glycol) diglycidyl ether (PEGDGE), 1-methyl-2-pyrrolidone (NMP), N,N-dimethylformamide (DMF, 99.9%), nafion 117 solution, acetonitrile (MeCN)(HPLC grade), tetraethyl orthosilicate (TEOS), 25% ammonia solution, hydrofluoric acid, 98% sulfuric acid, 2,2'-azobis(isobutyronitrile), 1-Vinylimidazole (≥99%), allylamine (≥99%), sodium dithionite, methanol and absolute ethanol were purchased from Sigma-Aldrich. Diethyl ether was purchased from Merck. Luminol was supplied from Fluka (Biochemika, Switzerland). MWCNTs (Ø = 6-13 nm, 2.5-20 μm length, >98 % carbon basis) were purchased from Sigma-Aldrich (MO, USA). All aqueous solutions were prepared with type I deionized water (DW) at 18 MΩ.cm (Veolia). High-purity oxygen and argon were purchased from Air Liquide (France).

2.2. Preparation of SiO_2 (silica) templates

Silica NPs were synthesized via the classical Stöber Method (Han et al., 2017). Briefly, 1 mL of TEOS, 50 mL of ethanol, 1 mL of DW, and 5 mL of ammonia solution were magnetically stirred in a flask at 250 rpm and 25 ^oC in a water bath. After 6 h, SiO_2 NPs were purified by twice centrifugation at 10000 rpm for 20 min. The sedimented SiO_2 NPs were resuspended in ethanol (Figure S1A), and the suspension was evaporated in an oven at 70 ^oC to obtain templates (Figure S1B).

2.3. Preparation of macroporous carbonaceous material (MC)

The precursor of carbonaceous material contains 1.4 g of sucrose, 3.2 mL of DW, 14 mL of ethanol, and 40 µL of 98% sulfuric acid. The infiltration was carried under the vacuum by dropping carbon precursor solution onto the silica template at room temperature. The infiltration was repeated several times to fill the voids of the silica template. The sucrose-soaked templates were heated at 160 °C for 5 h in the air for the carbonization of sucrose catalyzed by sulfuric acid. Macroporous carbon (MC) was left behind by etching away silica templates with 4% HF solution overnight (Figures 1 A and B).

2.4. Extraction and purification of PSII from spinach

PSII was obtained with minor modifications according to the reported method (van Leeuwen et al., 1991). Fresh and clean spinach leaves were ground in a blender in buffer A (20 mmol L^{-1} MES, pH 6.0, 15 mmol L^{-1} NaC1, 5 mmol L^{-1} $CaC1_2$, and protease inhibitor benzamidine) at 4 °C. The mixture was filtrated through the cloth and centrifuged for 10 min at 10,000 g. The chloroplast pellet was resuspended in buffer A to a concentration of 2 mg Chlorophyll (Chl) mL^{-1}, and triton X-100 was added to a concentration of 25 mg/mg Chl. After 15 min of gentle stirring, the suspension was centrifuged for 25 min at 40,000 g. The thylakoids were resuspended in buffer A supplemented with 0.4 mol L^{-1} sucrose, and the starch was separated by centrifugation at 2,000 g for 5 min and then at 40,000 g for 25 min. PSII was extracted and purified by resuspending the thylakoids in buffer B (20 mmol L^{-1} MES, pH 6.0, 20 mmol L^{-1} $MgCl_2$, 5 mmol L^{-1} $CaC1_2$, 10 mmol L^{-1} $MgSO_4$, 0.4 M sucrose and 0.6% n-Dodecyl β-D-maltoside) to a concentration of 2 mg Chl ml^{-1}. The suspension was gently stirred at room temperature for 10 min and sedimented for 20 min at 40,000 g to remove any non-soluble content. The supernatant was loaded (15 mL min^{-1}) onto a Q-Sepharose anion exchanger (Cytiva, 1 g Q-Sepharose per 1 mg Chl), and prewashed with buffer B, to purify PSII completely. The column was eluted with buffer B till the eluate turned into colorless aliquots at a flow rate of 0.5 column volume/min. PSII was removed from Q-Sepharose by stepwise increasing $MgSO_4$ concentration to 75 mmol L^{-1} (Figure S2A). PSII aliquots were concentrated at 2 mg Chl mL^{-1} using a 30,000 MWCO polysulfone centrifugal filter (Millipore) (Figure S2B) and stored at -77 ^{o}C before use. The extraction procedure was conducted on ice or at 4 °C by avoiding ambient illumination.

2.5. Synthesis of osmium complex

Firstly, $Os(bpy)_2Cl_2$ was synthesized following the previous study (Habermüller et al., 2000). Briefly, 2.2 mmol 2,2'-bipyridyl and 1mmol K_2OsCl_6 were mixed in 20 mL DMF and refluxed for 1 hour under stirring. Then the precipitated KCl was removed, and the mixture was transferred to the flask. 250 mL diethyl ether was added dropwise under stirring. Then the intermediate product was dissolved in 10 mL DMF and 5 mL methanol, and 1 g sodium dithionite in 100 mL DW was added to the mixture while stirring and put in an ice bath. The product was filtered and washed with DW, methanol, and ethanol. Product mass: 0.68 g. ^{1}H NMR (400 MHz, DMSO-D_6) : δ (ppm) = 8.57, (t, 2H); 7.66 (t, 2H); 7.39 (br. s, 2H); 7.07 (br. s, 2H); 6.93 (br.s, 2H); 5.32 (br.s, 2H); 3.32 (s, 4H); 2.67 (t, 2H); 2.50 (s, 4H); 2.33 (t, 2H); 1.24 (s, 4H); 1.06 (t, 2H); 0.86 (t, 2H). UV/Vis (DMF): 297 nm (3.69, π → π* bipyridyl), 385 nm (0.97, d → d Os^{2+}), 470 nm (0.90, d → d Os^{2+}), 560 nm (1.05, d → d Os^{2+}).

2.6. Synthesis of the polymer backbone and osmium polymer

Synthesis of the copolymer of vinylimidazole and allylamine was carried out according to the previous study (Badura et al., 2008)**.** In a typical experiment, 0.2 mL allylamine and 3 mL vinylimidazole was left to copolymerize by stirring under argon at 70 ^{o}C after adding 240 mg 2,2'-azobis(isobutyronitrile) as a free radical initiator. After 2 hours, the residue was dissolved in 6 mL absolute ethanol and then transferred to 60 mL acetone drop by drop under stirring. Finally, the product was washed with acetone and dried under vacuum. The copolymer contains 14.3% of allylamine and 85.7% of vinylimidazole, and the average molecular weight of the copolymer was calculated as 88.8 g mol^{-1} (product mass: 2.04 g). ^{1}H NMR (400 MHz, DMSO-D_6): δ (ppm) = 7.50–6.57 (36%, br.d, Im); 4.87 (s, H_2O); 3.75–3.24 (20%, br.q, H_2NCH_2, EtOH); 3.24-2.75 (42%, br.m, backbone $CHCH_2$); 1.06 (0.6%, t, EtOH); 1.18–1.09 (1%, br.s, CH_3).

The osmium polymer was produced by the coordinative binding of $Os(bpy)_2Cl_2$ to the polymer backbone, according to the literature (Badura et al., 2008).

2.7. Preparation of PSII immobilized and osmium polymer sensitized MC coated photoanodes (GCE|MC|Os polymer|PSII)

The glassy carbon electrodes (GCEs) (Ø = 3 mm and 0.071 cm^2) were cleaned by polishing with a 1 µm diamond paste (Presi, France) and sonicated successively in DW, acetone, and ethanol. MC was affixed to GCEs using Loctite conductive carbon ink (the Netherlands).

Then, the modification solution was prepared by mixing 30 µL of 2 mg mL^{-1} thawed PSII in buffer B (20 mmol L^{-1} MES, pH 6.0, 20 mmol L^{-1} $MgCl_2$, 5 mmol L^{-1} $CaC1_2$, 10 mmol L^{-1} $MgSO_4$, 0.4 mol L^{-1} sucrose and 0.6% n-Dodecyl β-D-maltoside), 10 µL of 5 mg mL^{-1} osmium complex polymer in DW and 4 µL PEGDGE. 16 µL of modification solution was drop-casted on the as-prepared carbonaceous surface. The modified GCEs were kept in the refrigerator at 4 °C for 24 h for cross-linking with PEGDGE and then rinsed with buffer to eliminate unbound content. Finally, nafion in methanol (0.5%) was deposited on the electrodes to preserve the surface, and the photobioanodes were stored at 4 °C when not in use.

2.8. Preparation of biocathodes

20 µL of a sonicated MWCNT dispersion in NMP (5 mg mL^{-1}) were drop-casted on cleaned GCEs. The hemin was attached to MWCNT-coated GCEs by drop-casting 15 µL of hemin (0.3 mmol L^{-1}) in DMF to orientate BOx. Finally, 20 µL of BOx solution in PBS pH:7 (5 mg mL^{-1}) was drop-casted and left at 4 °C overnight. The electrodes were rinsed with PBS, and the intact biocathode was defined as BOx/hemin-MWCNT/GCE.

2.9. Characterization, electrochemical and photoelectrochemical studies

For the electrochemical and photoelectrochemical experiments conducted in a three-electrode configuration cell in aqueous solutions, a GCE was utilized as a working electrode (Ø = 3 mm), an Ag/AgCl saturated with sat. KCl was used as the reference electrode, and a Pt wire was introduced as a counter electrode. The electrochemical studies in organic solvents were carried out in a glove box (under dry argon atmosphere, $[O_2]$ ≈100 ppm), and an $Ag/AgNO_3$ (10 mM in MeCN + 0.1 M ($[Bu_4N]PF_6$ as the supporting electrolyte) was used as a reference electrode. DMF was degassed by bubbling argon and dried over 3 Å molecular sieves (Sigma-Aldrich). All electrochemical studies were performed on an Autolab PGSTAT100 potentiostat/galvanostat operated by NOVA 2.1 software. NMR spectra were recorded on a Bruker AVANCE 400 operating at 400.0 MHz for 1H. The morphology of the MC was imaged by field emission scanning electron microscopy (FESEM) using an FEI Quanta 450 FEG operating at an accelerating voltage of 15 kV. UV-visible absorption spectra were obtained using a Perkin Elmer spectrophotometer (Lambda 650) with a quartz cell (1 cm length). Emission spectra were obtained in the deoxygenated solvent at ambient temperature

using Fluoromax 4 (Horiba). Raman spectrum was recorded on Zeiss EC Epiplan. Luminol power intensity was measured by Newport 2835-C Multi-Function Optical Meter. Beckman Coulter Ultracentrifuge Optima XPN-90 was used during PSII purification. The particle size distribution of silica NPs was obtained on a Nano Plus (Micromeritics).

The photobioanode was coupled to the biocathode to yield the respective PBFC by attaching the photobioanode to the counter and reference leads, and the biocathode to the working lead. The electrodes were immersed in PBS (0.1 mol L^{-1}, pH=7.4). A vial was fixed in the cell, where chemiluminescence (CL) reactions were carried out to separate the alkaline buffer.

The chemiluminescence conditions were followed according to the literature with some modifications (Golub et al., 2012). The photo-electrode was placed in a 10 mL measurement cell containing 500 μL of 10 mmol L^{-1} pH = 7.4 HEPES buffer containing 20 mmol L^{-1} KNO_3, 200 mmol L^{-1} $NaNO_3$, and 2 mg mL^{-1} GOx. Then, various concentrations of glucose were added. After 15 min, a 2.5 mL pH = 9.0 HEPES buffer containing 20 mmol L^{-1} KNO_3, 200 mmol L^{-1} $NaNO_3$, and 1 μmol L^{-1} hemin was mixed with the buffer. Eventually, luminol was introduced into the solution with a final concentration of 0.57 mmol L^{-1} to start the chemiluminescence and in turn the photocurrent generation.

Also, the visible-light-induced PEC performance of the photosensitive entities on the electrodes was investigated. For this purpose, the photobioanode was placed in an electrochemical cell and illuminated with the aid of optical fiber. A UV and IR cutoff filter below 420 nm and above 630 nm was utilized in the light source, and the light power was 11.2 mW cm^{-2}.

3. RESULTS AND DISCUSSION

3.1. Characterization, Electrochemical, and Spectrophotometric Studies

The schematic illustration of CL-triggered BFC assembly is shown in Scheme 1A. In the photobioanode, the electrons are transferred from PSII to Osmium complex polymer and then to MC-modified GCE by producing photocurrents under CL (Scheme 1B). The electron transfer rate of redox polymer depends on the flexibility, swelling feature, amount of cross-linking of the backbone, the distance between the backbone and the redox mediator, and the formal potential of the redox complex. To rule out the slow transfer rates and inefficient PSII loading, we chose one of the best PSII immobilization procedures in the literature to study PEC performance of PSII under CL. The PSII from spinach was purified as an active dimeric

subpopulation of PSII complexes with oxygen-evolving Mn_4CaO_5 cluster by yielding an oxygen evolution activity of 2640 µmol molecular oxygen per 116 µg Chl within 5 minutes ((Figure 1C and E; Figure 2A and B). The microscope and FESEM image of MC exhibit a highly porous morphology (Figure 1A and B). Nafion was coated as the outer layer to prevent the leakage of immobilized entities. The transition metal complexes can be used as a mediator and photosensitizer in the same system, which makes them favorable for PEC systems (Tel-Vered et al., 2010). In this study, Os complex was used for its versatile functions (Figure 1F). The luminol CL bestows the PBFC with "cold light" utilization, which is not harmful to the enzymes like UV radiation and does not cause enzyme denaturation like IR radiation. The thin layer chromatogram of PSII exhibits red fluorescence under UV light, typical of porphyrin rings in PSII (Figure 1D).

In the UV–visible spectrum in DMF (Figure 3A), the intense band at 297 nm can be attributed to the ligand-to-ligand charge transfer (LLCT, π-π* transition) of Os polypyridyl complexes. Os $(bpy)_2$ Cl_2 displayed the metal-centered (MC) transition at 385 nm and metal-to-ligand-charge transfer transitions (MLCT) at 470 nm, 560 nm (Wehlin et al., 2020). Upon the excitation at 470 nm, the Os complex displayed emissions bands at 503 and 545 nm implying small Stokes shifts arising from the ^{3}MLCT excited state (Figure 3B). The photocurrent generation is linearly proportional to the absorption intensity of PSII around two absorption bands centered at 425 nm and 675 nm (Figure 3C) (Kato et al., 2014; Yehezkeli et al., 2012). The former is the Soret or B-band, and the latter is termed the Q-bands of porphyrins in PSII. The Q-bands originate from the transition from the ground state to the first excited state. The Soret absorption stems from the electron transition from the ground state to the second excited state, which makes this band lie in the blue region (Senge et al., 2014).

The luminol CL emission spectrum reveals a sharp band centered at 425 nm (Figure 3C). It can be a potential candidate for PSII excitation since the emission spectrum nearly overlaps with the main absorption band of PSII. Therefore, PSII can be used as a sensitizer for the CL-triggered PEC systems and can lead to unprecedented photon-to-current efficiency for PSII.

In Figure 3D, the Raman spectrum of MC revealed the G band at 1587 cm^{-1} corresponding to the E_2g phonon of sp^2 C atoms and the D band at 1357 cm^{-1}, which is attributed to A_1g breathing mode of κ-point phonons. The D band stems from defects such as grain boundaries, vacancies, and amorphous carbon species (Id/Ig =1.00). The broad band centered at 2754 cm^{-1} is the combination of 2D and (D+G) bands, indicating the graphitization with some defects.

Slow-scan cyclic voltammograms (CV) were obtained to elucidate the electrochemical features of Os $(bpy)_2Cl_2$ in DMF (Figure 4A). In the anodic part, the CV displays reversible oxidation at $E^{ox}_{1/2}$ = 0.46 V, corresponding to the metal-centered Os(III)/Os(II) redox system. Three successive reversible peak systems at $E^{red}_{1/2}$ = -1.75 V, -2.11 V, and -2.3 V vs. $Ag/AgNO_3$ correspond to the one-electron reduction of the bipyridine ligand (Büldt et al., 2015; Le Goff et al., 2011).

The band gap energy (E_g), the highest occupied molecular orbital (HOMO), and the lowest unoccupied molecular orbital (LUMO) energy levels were calculated using the following equations(Çakıroğlu et al., 2020):

$$E_{HOMO}(eV) = -e(E_{ox} + 4.80) \qquad (1)$$

$$E_{LUMO}(eV) = -e(E_{red} + 4.80) \qquad (2)$$

$$E_g(eV) = E_{LUMO} - E_{HOMO} \qquad (3)$$

E_{ox} and E_{red} are the onset potentials of oxidation and reduction, respectively. -4.8 eV is the $Ag/AgNO_3$ potential versus vacuum. HOMO and LUMO energy levels are found to be -5.6 eV and -2.92 eV, respectively. Also, the band gap energy was calculated as 2.68 eV (≈ 463 nm). The HOMO level of Os polymer is more negative than that of PSII, which implies a thermodynamic driving force for electron transfer from PSII. Also, the CV of the photobioanode demonstrated a redox curve with an E_{ox} of 80 mV due to the Os(II/III) transitions. In the enzyme electrodes, osmium polypyridinyl complexes are suitable mediators and photosensitizers for PSII-catalyzed water oxidation due to their appropriate oxidizing potentials.

Furthermore, the CV was recorded in 0.1 M PBS at pH 7.4 to interrogate the accessibility of the Os complex (Figure 4B). Although the CV of MC-coated GCE revealed no redox curve, the CV of Os complex-coated GCE displayed a well-defined redox process for the one-electron reduction of the bipyridine ligand. The $E_{1/2}$ value was calculated as 0.04 V vs. Ag/AgCl with the peak-to-peak separation (ΔE_P) of 0.08 V. Narrow ΔE_P implies fast electron transfer with high reversibility of the redox system, and Os complex polymer led to reduced diffusion issues, electron tunneling distance, and resistivity.

3.2. Photoinduced charge transfer

The photogenerated electron transportation was shown in Scheme 1B. The location of the photosensitive entities, which are Os complex and PSII, is of great importance to enhance the photogenerated charge carrier separation and transfer. Therefore, the appropriate position of the HOMO and LUMO levels of the Os complex with regard to the energy levels of PSII must be taken into consideration. Upon concurrent photoexcitation of both PSII and Os complex by chemiluminescence, the valence band (VB) electrons of PSII are excited to the conduction band (CB), creating electron holes in VB. Since the Soret band energy level (CB) of porphyrin within PSII is more positive than the LUMO energy level of the Os complex (Chen et al., 2017; Liang et al., 2013), the photogenerated electrons thermodynamically move to the Os complex polymer and then to the underlying MC, which serves as an electron trap for photoinduced electrons and migrate to the biocathode, where O_2 is reduced to H_2O by BOx by producing electricity. Water oxidation continuously provides electrons for the hole-scavenging process at VB of PSII. Herein, MC is an electron collector and thus reduces the possibility of photogenerated electrons falling back to the hole called "recombination" by leading to efficient photogenerated charge separation. The distance between the energy levels of photosensitive entities is different enough to accomplish an efficient staircase shape photogenerated electron transfer, called the "Type II" mechanism.

Figure 4C shows the effect of the applied potential on the photocurrent generation under visible light in PBS. At potentials higher than 0 V vs. Ag/AgCl, the relay unit Os(II) undergoes two successive one-electron oxidations to form Os(III) acceptor state, which is prone to reduction to Os(II) by PSII (Figure 4C, curve a). Finally, the photogenerated charge convey is achieved by directly injecting the electrons from Os(II) to MC and GCE by turning to Os(III). Thus, the vectorial electron convey diminishes the back electron transfer and enhances the photocurrent generation (Yehezkeli et al., 2012). However, at potentials lower than 0 V, the photocurrents sharply reduced since the relay units constantly remain in the reduced Os(II) state that does not accept the electrons from the PSII, and the photo-induced electrons end up annihilating by the electron-hole recombination. On the other hand, Os polymer-coated electrode without PSII yielded negative photocurrents at potentials lower than 0 V (Figure 4C, curve b), confirming that PSII immobilization rendered the electrode bioanode even for low potentials.

At 0 V vs. Ag/AgCl, a photocurrent of 707 nA cm^2 was observed at the photobioanode. Miyachi et al. combined PSII (from *Thermosynechococcus elongatus*) with trimethyl benzoquinone-modified Pt NPs and immobilized the mixture on gold electrodes. At 0.10 V vs.

Ag/AgCl (under 680 nm irradiation, P = 29 mW cm^{-2}), the photocurrent was 15 nA cm^{-2} (Miyachi et al., 2017). Cai et al. used an ITO-PEI-rGO/PSII (from spinach) at 0.25 V vs. SCE and found a photocurrent of 37.2 nA cm^{-2} under light illumination (800 nm > λ >550 nm, P_{680nm}=10 mW cm^{-2})(Cai et al., 2015). Li et al. fabricated ITO/PPyBQ/PSII (from spinach) electrode, and at 0.25 V versus SCE, the photocurrent was found to be 360 nA cm^{-2} under light illumination (800 nm > λ >550 nm, P_{680nm}=10 mW cm^{-2})(Li et al., 2017). Kato et al. immobilized PSII (from *T. elongatus*) onto carboxylate-functionalized mesoporous ITO. At 0.5 V vs. NHE, the photocurrent was 430 nA cm^{-2} after the covalent binding of PSII, while a photocurrent of 280 nA cm^{-2} was found upon electrostatic orientation(Kato et al., 2013). Yehezkeli et al. immobilized PSII (from *Mastigocladus Laminsus*) on poly-benzyl viologen redox polymer modified ITO electrode as a bi-layer assembly $(PBV^{2+}/PSII)_2$ and observed a photocurrent of 500 nA cm^2 at 0 V vs. Ag/AgCl (Yehezkeli et al., 2013). According to the literature, PSII activity and stability are directly related to biological resources. The redox polymers and mediators have also substantially facilitated the electron transfer from PSII to the electrode surface and led to boosted photocurrent generations compared to metal NPs and regular polymers. The highest photocurrent values for PSII were achieved in the semiconducting support materials such as mesoporous indium tin oxide and titanium dioxide or photosensitive matrix entities such as osmium complex modified redox polymers. Especially mesoporous indium tin oxide yielded very satisfying photocurrents for PSII due in part to the porous architecture, which leads to abundant PSII immobilization (Kato et al., 2012). In this study, a good PEC performance was observed due to the supply of light energy with perfect emission spectrum for PSII, porous morphology of electron trapping carbon material, and PEC behavior of osmium polymer. Also, spinach is a cheap resource for PSII extraction compared to cyanobacteria, which request special cell growth conditions along with time-consuming procedures.

The open circuit potential (V_{OC}) of BFCs has been enhanced by fabricating biocathodes with high O_2 reduction potentials. BOx is an advantageous enzyme for reducing O_2 to H_2O at the biocathodes due to its favorable biocatalytic activity and less liability to chloride ions at the physiological medium. In Figure 4D, the CVs of the biocathode revealed DET owing to the oriented immobilization of BOx. In the oxygen-saturated buffer, a steeper cathodic catalytic wave with an initial potential of 0.54 V vs. Ag/AgCl was observed. The experimental oxidation potential is consistent with the DET potential of oxygen reduction via one-proton-coupled one-electron transfer by BOx (Lalaoui et al., 2015). The observed half-wave potential

was 0.5 V vs. Ag/AgCl and close to the redox potential of the T1 copper center of BOD from Mv (0.43 V vs. SCE at pH 7) (Lalaoui et al., 2015) and thermodynamically reduce O_2 to H_2O due to more positive potential of O_2/H_2O (0.572 V vs. SCE at pH 7.0) (Gross et al., 2017). Also, the intimate contact between BOx and MWCNTs led to a satisfying O_2 reduction current.

3.3. Biosensing performance of PBFC

The power studies of the PBFC assembly were carried out by placing the electrodes (the bioanode and the biocathode) in parallel with a short distance of 1.5 mm, which reduces the electrolyte resistance and current loss. The cell was covered with aluminum foil to keep the CL inside, and the membraneless H_2O/O_2 PBFC was manufactured. The manufactured PBFC eliminates the need for additional electron donor species.

Figure 5A exhibits the OCP vs. glucose concentration graph. The OCPs increased with the increasing light power intensity and then leveled off. Previous reports also confirmed this phenomenon (Seitkhan et al., 2020; Xiao et al., 2018). The CL-triggered PBFC delivered an OCP of 0.531 V in 30 mmol L^{-1} glucose. The calibration curve was obtained from the linear part of the graph (Figure 5B), and the regression equation was found to be P (V) = 0,019 $C_{glucose}$ (mmol L^{-1}) + 0,383 (R^2 = 0,994). The sensitivity was found to be 19 mV L $mmol^{-1}$ cm^{-2}. The limit of detection (LOD) was calculated as 16.5 µmol L^{-1} based on 3x (standard deviation of 10 blank measurements/sensitivity), and the limit of quantification was found to be 55 µmol L^{-1} based on 10x (standard deviation of 10 blank measurements/sensitivity).

Five photobioanodes manufactured from the same batch revealed satisfying reproducibility with a relative standard deviation (RSD) of 3.3%, implying good reproducibility.

Ascorbic acid, uric acid, D-lactose, D-maltose, D-mannitol, and galactose can be found in the biological media as interfering substances during glucose detection. The addition of 0.5 mmol L^{-1} of each interfering substances to the 5 mmol L^{-1} glucose-containing buffer exhibited 5.4% reduction in OCP compared to the initial response (Figure S3), implying acceptable selectivity.

The storage stabilities of the electrodes were studied at a mild fixed potential of 0.2 V by measuring the currents. After ten days, 96% and 93% of their initial current outputs remained for photobioanode and biocathode, respectively. The good stability is probably due to the robust architecture of the electrode materials with intimate contact between the components and proves the electrodes' feasibility for the fast and stably responsive PBFC construction.

CONCLUSIONS

Herein, the blue sideband (Soret) of PSII was excited for the first time by luminol chemiluminescence in a biofuel cell type PEC system, and PSII was used as a photosensitizer for sensitive and selective enzymatic glucose detection without an external power source. The concomitant production of H_2O_2 and gluconic acid out of glucose by GOx allows to correlate photocurrent and glucose concentration. The blue sideband of PSII with a high IPCE perfectly overlapped with the emission spectrum of chemiluminescence by leading to efficient light harnessing, which was observed by a substantial amount of oxygen and photocurrent generation. Os polymer matrix provided efficient wiring, and good electrical contact and macroporous carbon enabled high loading of both Os polymer and PSII. The OCPs have increased proportional to the CL power intensity, in turn, glucose concentration in the range of 0-6 mmol L^{-1}. PSII can be an incomparable photosensitizer in PEC systems to capture and convert CL light efficiently, and the feasibility can be improved by enhancing the stability with enzyme engineering. The present PBFC may extend the insight beyond the conventional PEC biosensing systems in the future.

Acknowledgments

The study is dedicated to Grenoble earning the “2022 European Green Capital” title. The French National Centre for Scientific Research (CNRS) and Sakarya University Scientific Research Projects Unit (Project No: 2022-16-36-21) are acknowledged for the research budget. We are very grateful to CNRS Eng. Yannig Nédellec for his assistance, Assoc. Prof. Emrah Bulut for assistance with FESEM imaging, and Dr. Yavuz Derin for obtaining emission spectra.

References

Badura, A., Guschin, D., Esper, B., Kothe, T., Neugebauer, S., Schuhmann, W., Rögner, M., 2008. Photo-induced electron transfer between photosystem 2 via cross-linked redox hydrogels. Electroanalysis 10, 1043–1047.

Büldt, L.A., Prescimone, A., Neuburger, M., Wenger, O.S., 2015. Photoredox Properties of Homoleptic d6 Metal Complexes with the Electron-Rich 4,4′,5,5′-Tetramethoxy-2,2′-

bipyridine Ligand. Eur. J. Inorg. Chem. 2015, 4666–4677.

Cai, P., Feng, X., Fei, J., Li, G., Li, Jiao, Huang, J., Li, Junbai, 2015. Co-assembly of photosystem II/reduced graphene oxide multilayered biohybrid films for enhanced photocurrent. Nanoscale 7, 10908–10911.

Çakıroğlu, B., Chauvin, J., Le Goff, A., Gorgy, K., Özacar, M., Holzinger, M., 2020. Photoelectrochemically-assisted biofuel cell constructed by redox complex and g-C3N4 coated MWCNT bioanode. Biosens. Bioelectron. 169, 112601.

Chen, C., Gong, N., Li, Z., Sun, C., Men, Z., 2017. Concentration Effect on Quenching of Chlorophyll a Fluorescence by All-Trans-β-Carotene in Photosynthesis. Molecules.

Cosnier, S., Gross, A.J., Le Goff, A., Holzinger, M., 2016. Recent advances on enzymatic glucose/oxygen and hydrogen/oxygen biofuel cells: Achievements and limitations. J. Power Sources.

Dilbeck, P.L., Bao, H., Neveu, C.L., Burnap, R.L., 2013. Perturbing the Water Cavity Surrounding the Manganese Cluster by Mutating the Residue D1-Valine 185 Has a Strong Effect on the Water Oxidation Mechanism of Photosystem II. Biochemistry 52, 6824–6833.

Fang, X., Sokol, K.P., Heidary, N., Kandiel, T.A., Zhang, J.Z., Reisner, E., 2019. Structure–Activity Relationships of Hierarchical Three-Dimensional Electrodes with Photosystem II for Semiartificial Photosynthesis. Nano Lett. 19, 1844–1850.

Golub, E., Niazov, A., Freeman, R., Zatsepin, M., Willner, I., 2012. Photoelectrochemical biosensors without external irradiation: Probing enzyme activities and DNA sensing using Hemin/G-quadruplex-stimulated chemiluminescence resonance energy transfer (CRET) generation of photocurrents. J. Phys. Chem. C 116, 13827−13834.

Gratzel, M., Evans, M.C.W., Seibert, M., 1990. Photoelectrochemical Responses of Photo-System Ii Particles Immobilized on Dye- Derivatized 5, 379–389.

Gross, A.J., Chen, X., Giroud, F., Abreu, C., Le Goff, A., Holzinger, M., Cosnier, S., 2017. A High Power Buckypaper Biofuel Cell: Exploiting 1,10-Phenanthroline-5,6-dione with FAD-Dependent Dehydrogenase for Catalytically-Powerful Glucose Oxidation. ACS Catal. 7, 4408–4416.

Gross, A.J., Holzinger, M., Cosnier, S., 2018. Buckypaper bioelectrodes: Emerging materials for implantable and wearable biofuel cells. Energy Environ. Sci. 11, 1670–1687.

Habermüller, K., Ramanavicius, A., Laurinavicius, V., Schuhmann, W., 2000. An Oxygen-Insensitive Reagentless Glucose Biosensor Based on Osmium-Complex Modified Polypyrrole. Electroanalysis 12, 1383–1389.

Han, Y., Lu, Z., Teng, Z., Liang, J., Guo, Z., Wang, D., Han, M.Y., Yang, W., 2017. Unraveling the growth mechanism of silica particles in the stöber method: In situ seeded growth model. Langmuir 33, 5879–5890.

Hasan, K., Dilgin, Y., Emek, S.C., Tavahodi, M., Åkerlund, H.E., Albertsson, P.Å., Gorton, L., 2014. Photoelectrochemical communication between thylakoid membranes and gold electrodes through different quinone derivatives. ChemElectroChem 1, 131 – 139.

Heller, A., Feldman, B., 2008. Electrochemical glucose sensors and their applications in diabetes management. Chem. Rev.

Kato, M., Cardona, T., Rutherford, A.W., Reisner, E., 2013. Covalent immobilization of oriented photosystem II on a nanostructured electrode for solar water oxidation. J. Am. Chem. Soc. 135, 10610–10613.

Kato, M., Cardona, T., Rutherford, A.W., Reisner, E., 2012. Photoelectrochemical Water Oxidation with Photosystem II Integrated in a Mesoporous Indium−Tin Oxide Electrode. J. Am. Chem. Soc. Commun. 134, 8332−8335.

Kato, M., Zhang, J.Z., Paul, N., Reisner, E., 2014. Protein film photoelectrochemistry of the water oxidation enzyme photosystem II. Chem. Soc. Rev. 43, 6475–6660.

Lalaoui, N., Le Goff, A., Holzinger, M., Cosnier, S., 2015. Fully Oriented Bilirubin Oxidase on Porphyrin-Functionalized Carbon Nanotube Electrodes for Electrocatalytic Oxygen Reduction. Chem. – A Eur. J. 21, 16868–16873.

Le Goff, A., Holzinger, M., Cosnier, S., 2011. Characterization of multi-walled carbon nanotube electrodes functionalized by electropolymerized tris(pyrrole-ether bipyridine) ruthenium (II). Electrochim. Acta 56, 3633–3640.

Li, G., Feng, X., Fei, J., Cai, P., Li, Jiao, Huang, J., Li, Junbai, 2017. Interfacial Assembly of Photosystem II with Conducting Polymer Films toward Enhanced Photo-Bioelectrochemical Cells. Adv. Mater. Interfaces 4, 1600619.

Liang, Y., Bradler, M., Klinger, M., Schalk, O., Balaban, M.C., Balaban, T.S., Riedle, E., Unterreiner, A.-N., 2013. Ultrafast Dynamics of meso-Tetraphenylmetalloporphyrins: The Role of Dark States. Chempluschem 78, 1244–1251.

Miyachi, M., Ikehira, S., Nishiori, D., Yamanoi, Y., Yamada, M., Iwai, M., Tomo, T., Allakhverdiev, S.I., Nishihara, H., 2017. Photocurrent Generation of Reconstituted Photosystem II on a Self-Assembled Gold Film. Langmuir 33, 1351–1358.

Neveu, C.L.,. Https://en.wikipedia.org/wiki/File:PhotosystemII.PNG. 01.07.2022.

Riedel, M., Parak, W.J., Ruff, A., Schuhmann, W., Lisdat, F., 2018. Light as Trigger for Biocatalysis: Photonic Wiring of Flavin Adenine Dinucleotide-Dependent Glucose Dehydrogenase to Quantum Dot-Sensitized Inverse Opal TiO2 Architectures via Redox Polymers. ACS Catal. 8, 5212–5220.

Seitkhan, A., Neophytou, M., Hallani, R.K., Troughton, J., Gasparini, N., Faber, H., Abou-hamad, E., Hedhili, M.N., Harrison, G.T., Baran, D., Tsetseris, L., Anthopoulos, T.D., Mcculloch, I., 2020. A Multilayered Electron Extracting System for Efficient Perovskite Solar Cells. Adv. Funct. Mater. 30, 2004273.

Senge, M.O., Ryan, A.A., Letchford, K.A., MacGowan, S.A., Mielke, T., 2014. Chlorophylls,

Symmetry, Chirality, and Photosynthesis. Symmetry (Basel). 6, 781–843.

Sokol, K.P., Mersch, D., Hartmann, V., Zhang, J.Z., Nowaczyk, M.M., Rögner, M., Ruff, A., Schuhmann, W., Plumeré, N., Reisner, E., 2016. Rational wiring of photosystem II to hierarchical indium tin oxide electrodes using redox polymers. Energy Environ. Sci. 9, 3698–3709.

Tarakanov, I.G., Tovstyko, D.A., Lomakin, M.P., Shmakov, A.S., Sleptsov, N.N., Shmarev, A.N., Litvinskiy, V.A., Ivlev, A.A., 2022. Effects of Light Spectral Quality on Photosynthetic Activity, Biomass Production, and Carbon Isotope Fractionation in Lettuce, Lactuca sativa L., Plants. Plants 11.

Tel-Vered, R., Yildiz, H.B., Yan, Y.-M., Willner, I., 2010. Plugging into Enzymes with Light: Photonic "Wiring" of Enzymes with Electrodes for Photobiofuel Cells. Small 6, 1593–1597.

Van Leeuwen, P.J., Nieveen, M.C., van de Meent, E.J., Dekker, J.P., van Gorkom, H.J., 1991. Rapid and simple isolation of pure photosystem II core and reaction center particles from spinach. Photosynth. Res. 28, 149–153.

Wang, P., Zhao, F., Hartmann, V., Nowaczyk, M.M., Ruff, A., Schuhmann, W., Conzuelo, F., 2020. Reassessing the rationale behind herbicide biosensors: The case of a photosystem II/redox polymer-based bioelectrode. Bioelectrochemistry 136, 107597.

Wehlin, S.A.M., Troian-Gautier, L., Maurer, A.B., Brennaman, M.K., Meyer, G.J., 2020. Photophysical characterization of new osmium (II) photocatalysts for hydrohalic acid splitting. J. Chem. Phys. 153, 54307.

Xiao, J., Chen, Z., Zhang, G., Li, Q., Yin, Q., 2018. Efficient device engineering for inverted non-fullerene organic solar cells with low energy loss †. J. Mater. Chem. C Table 6, 4457–4463.

Yehezkeli, O., Tel-Vered, R., Michaeli, D., Nechushtai, R., Willner, I., 2013. Photosystem i

(PSI)/Photosystem II (PSII)-based photo-bioelectrochemical cells revealing directional generation of photocurrents. Small 9, 2970–2978.

Yehezkeli, O., Tel-vered, R., Wasserman, J., Trifonov, A., Michaeli, D., Nechushtai, R., Willner, I., 2012. Integrated photosystem II-based photo-bioelectrochemical cells. Nat. Commun. 3, 742–747.

Zammit, E.M., Barbante, G.J., Carlson, B., Doeven, E.H., Barnett, N.W., Hogan, C.F., Richter, M.M., Francis, P.S., 2012. Chemiluminescence from osmium(ii) complexes with phenanthroline, diphosphine and diarsine ligands. Analyst 137, 2766–2769.

Zhang, J.Z., Reisner, E., 2020. Advancing photosystem II photoelectrochemistry for semi-artificial photosynthesis. Nat. Rev. Chem. 4, 6–21.

Zhang, L., Bai, L., Xu, M., Han, L., Dong, S., 2015. High performance ethanol/air biofuel cells with both the visible-light driven anode and cathode. Nano Energy 11, 48–55.

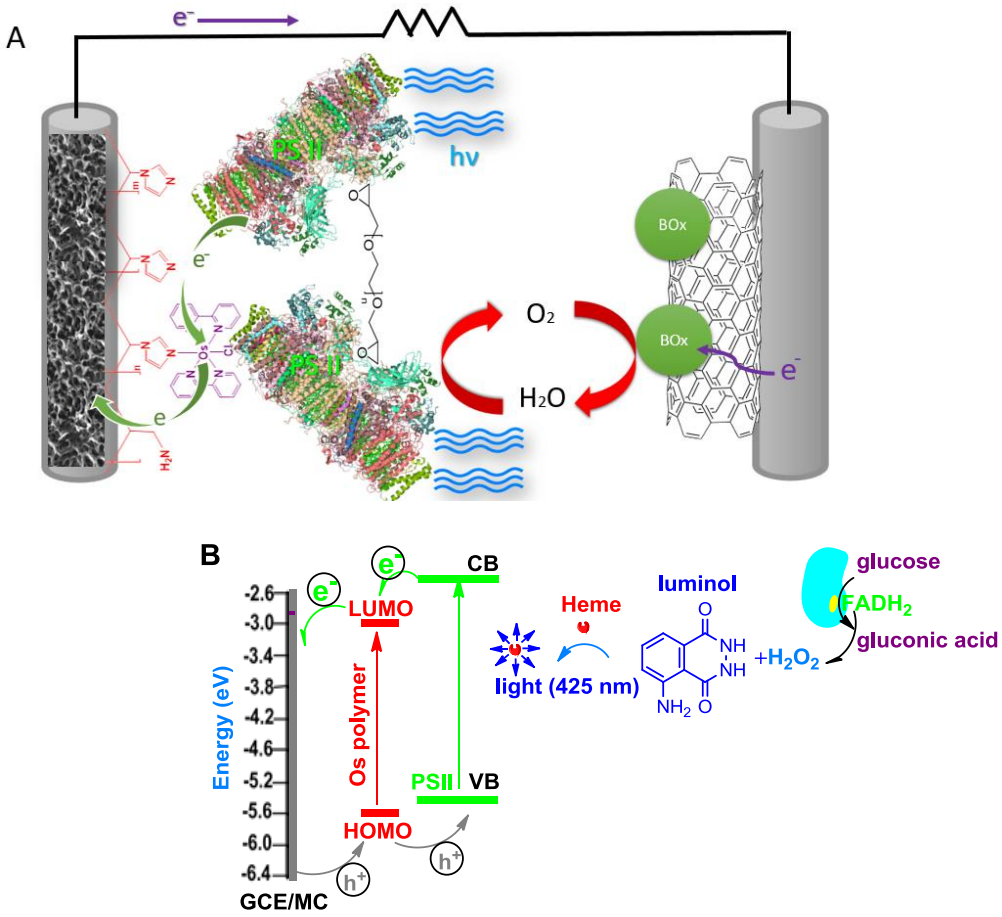

Scheme 1. Schematic of specially designed PBFC (A)(PSII image by courtesy of (Neveu, 2022)) and CL-triggered electron transfer with the energy levels of photoactive components (B)

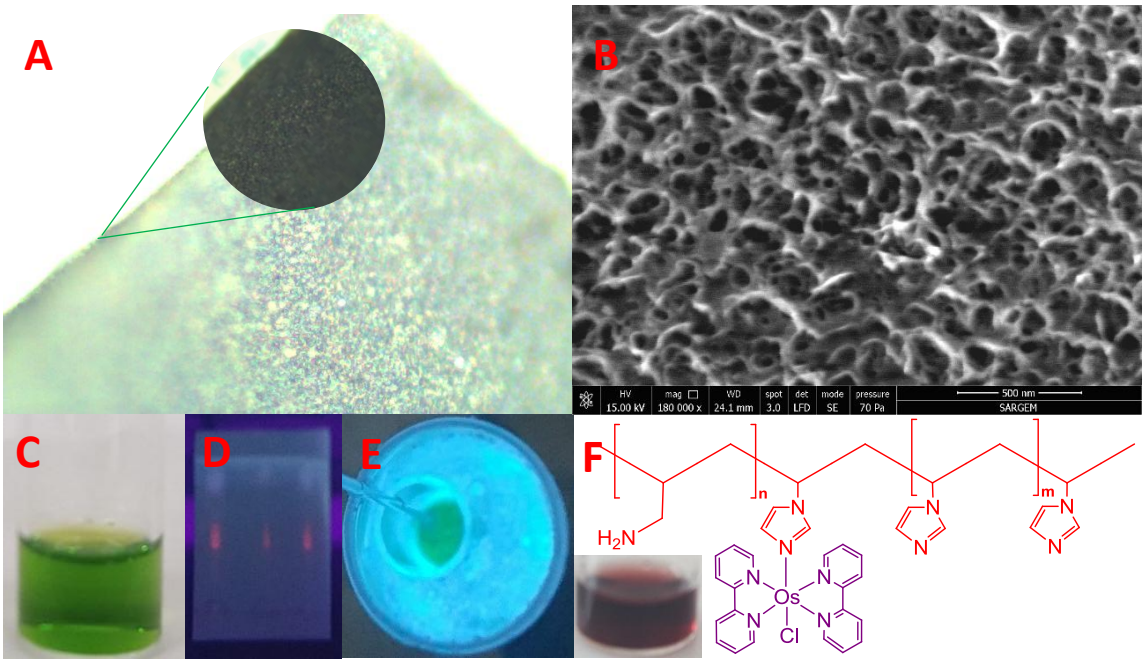

Figure 1. Microscope (A) and FESEM image of MC (B); PSII with vivid green color in buffer (C); Thin layer chromatogram of PSII (D); Sensing of O_2 release from PSII excited by CL (E); Os polymer structure (F)(inset shows Os complex solution)

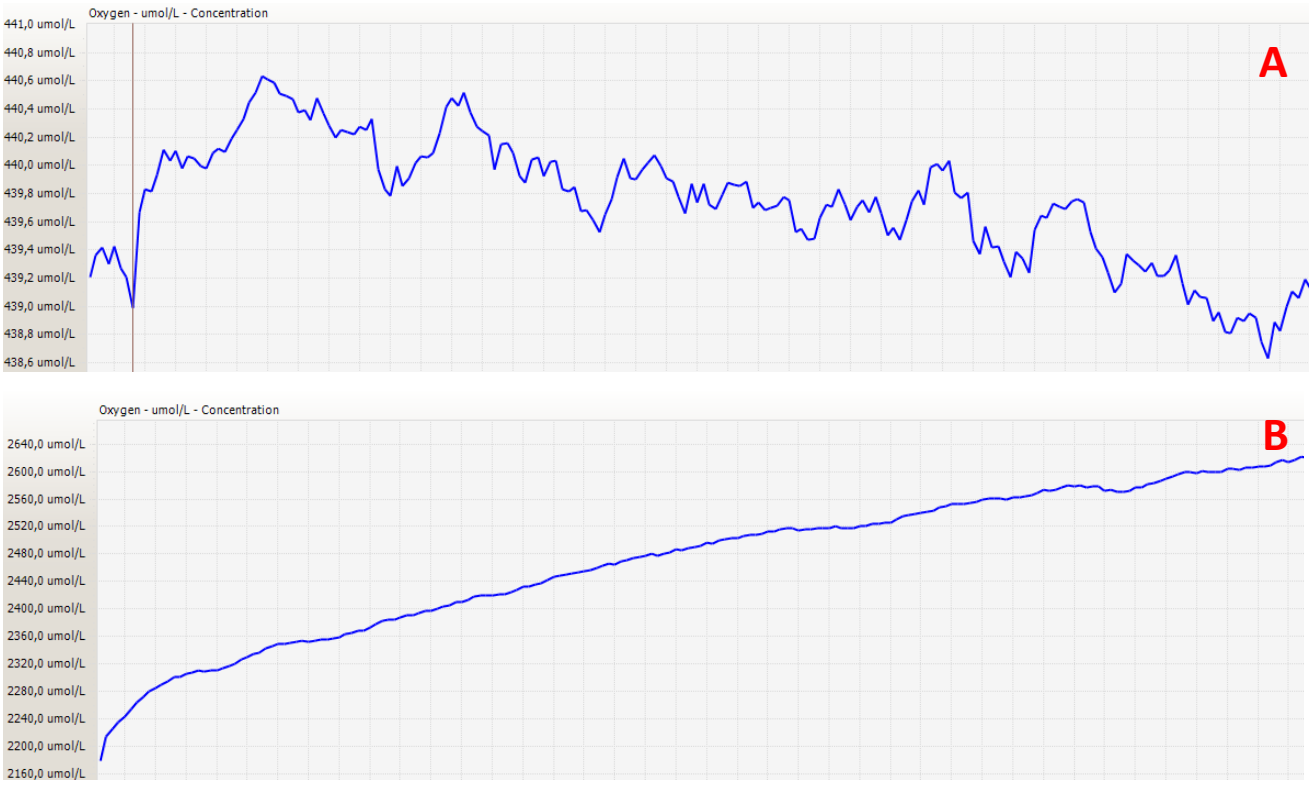

Figure 2. Oxygen concentration of buffer containing PSII before (A) and after CL (B)

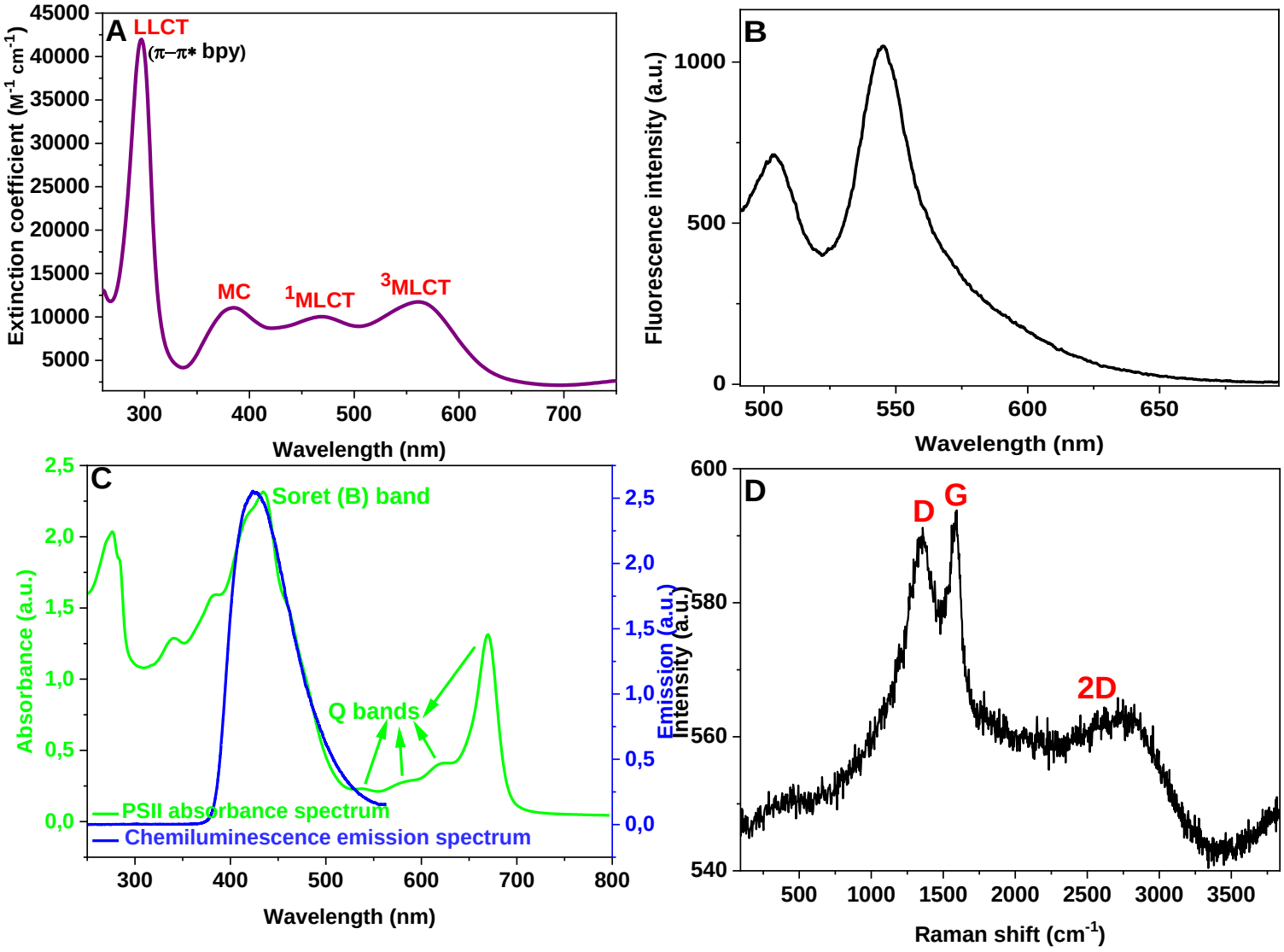

Figure 3. UV-vis absorbance (A) and fluorescence (B) spectrum of Os complex in degassed DMF ($Os(bpy)_2Cl_2$ concentration= 1.10^{-5} M); PSII absorption and luminol CL emission spectra (C); Raman spectrum of macroporous carbon (D)

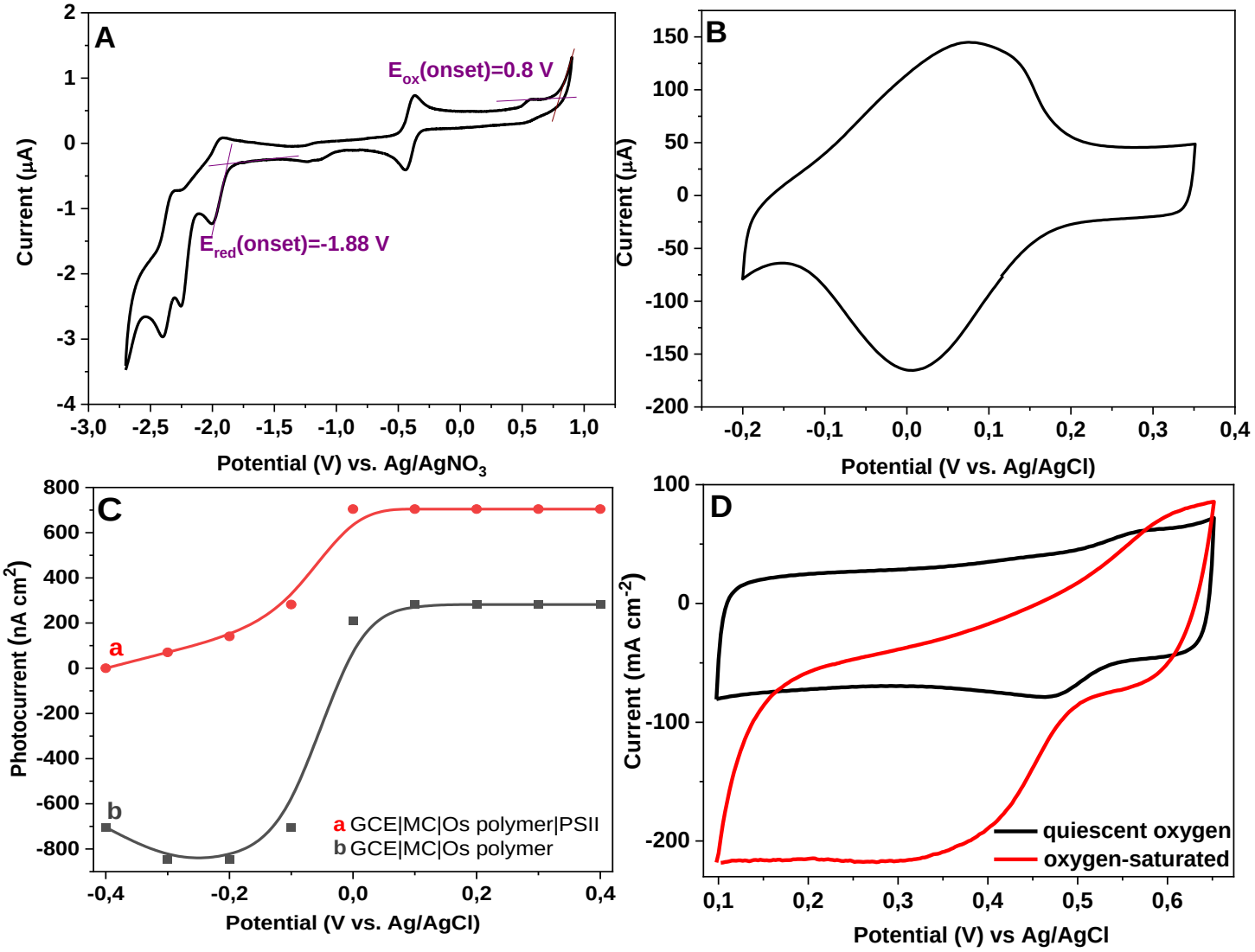

Figure 4. CV of 1 mmol L^{-1} Os $(bpy)_2Cl_2$ recorded at GCE (υ= 2 mV.s^{-1}) in deoxygenated DMF+0.1 M $[Bu_4N]PF_6$ (A); CV of GCE|MC|Os polymer (υ= 100 mV s^{-1}) in 0.1 mol L^{-1} PBS, pH 7.4 (B); The influence of external potential on the photocurrents generated by GCE|MC|Os polymer|PSII (a) and GCE|MC|Os polymer (b) under visible light illumination (P=11.2 mW cm^2, λ= 420-630 nm)(C); CVs of the GCE|MWCNT|BOx without and with oxygen-saturated 0.1 mol L^{-1} PBS pH 7.4 (D)

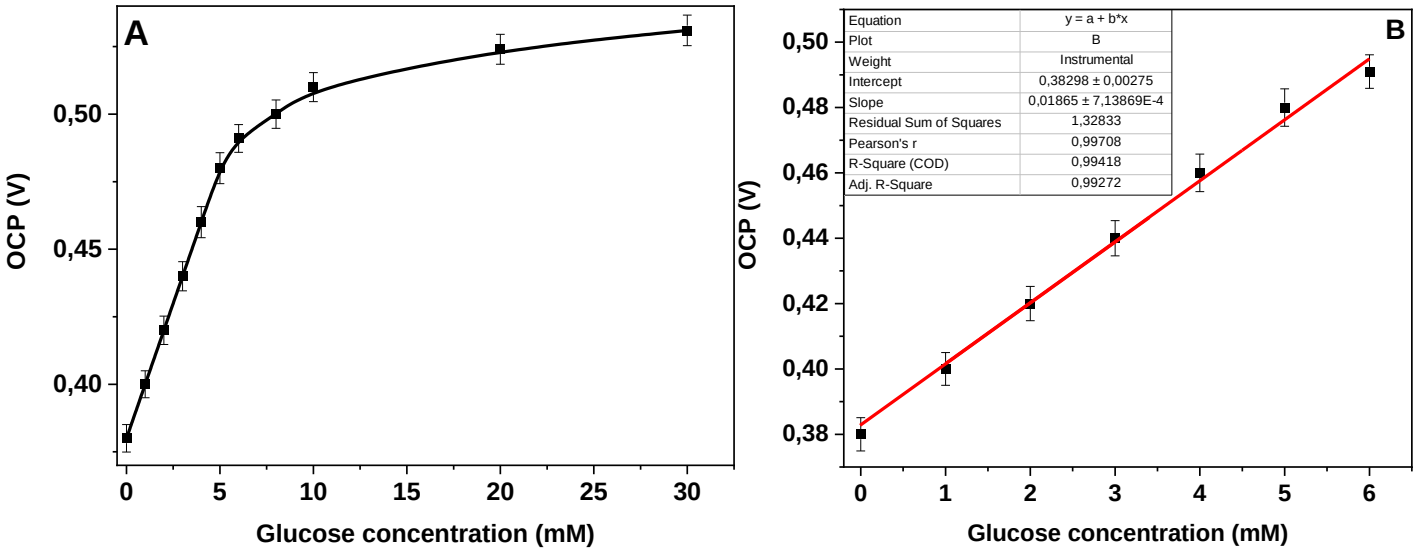

Figure 5. The dependence of OCPs on varying glucose concentrations under CL (A); Linear part of the plot (B) (Experiments were run in triplicate (n=3))